PCCP

Accepted Manuscript

ROYAL SOCIETY OF CHEMISTRY

www.rsc.org/pccp

Car – Parrinello and Path Integral molecular dynamics study of the intramolecular hydrogen bonds in the crystals of benzoylacetone and dideuterobenzoylacetone

Piotr Durlak*, Zdzisław Latajka

Faculty of Chemistry, University of Wrocław, 14 F. Joliot-Curie Str., 50-383 Wrocław, Poland.

Abstract

The dynamics of the intramolecular short hydrogen bond in the molecular crystal of benzoylacetone and its deuterated analogue are investigated using *ab initio* molecular dynamics simulations. A study on intramolecular hydrogen bonding in 1-phenyl-1,3-butadione **(I)** and 1-deuteroxy-2-deutero-1-phenylbut-1-en-3-one **(II)** crystals has been carried out at 160 K and 300 K on the CPMD method level and at 300 K on the PIMD method level. The analysis of the two-dimensional free-energy landscape of reaction coordinate δ-parameter and $R_{O...O}$ distances shows that the hydrogen (deuter) between the two oxygen atoms adopts slightly asymmetrically position in the single potential well. When the nuclear quantum effects are taken into account very large delocalization of bridging proton is observed. These studies indicate that the hydrogen bonds in the crystal of benzoylacetone have characteristic properties for the type of bonding model resonance assisted hydrogen bonds (RAHB) without existing equilibrium of the two tautomers. The infrared spectrum has been calculated, and a comparative vibrational analysis has been performed. CPMD vibrational results appear to qualitatively agree with the experimental ones.

Keywords

Hydrogen bond (HB), benzoylacetone (BA), dideuterobenzoylacetone (D_2BA), path integrals molecular dynamics (PIMD), proton transfer (PT), quantum effects, IR spectra, resonance assisted hydrogen bond (RAHB).

1. Introduction

The hydrogen bond is the most important of all directional intermolecular interactions [1]. We can distinguish several groups of hydrogen bonds due to their properties. Most often we share hydrogen bonds on the three main classes: strong, moderate and weak. Among the listed classes, the most important parameters are the length and angle of the bond, the energy of the bond, the position of the proton in the hydrogen bridge and the IR frequency shift of X-H stretching vibration. The most common classification of H bonds is the Jeffrey's [2] classification. Proton transfer and hydrogen bonds are fundamental for the function, stability, structure and dynamics of chemically and biologically relevant system. Very strong hydrogen bonds are among the most interesting features of hydrogen bond categories which have essential roles in biochemical reaction and enzyme catalysis as transition state [3, 4]. In some

specific molecular systems, for example: amides [5, 6], ketones [7], pyrroles [8], phenols [9], proteins and nucleic acids [10] the π-bond cooperativity phenomena were observed. These effects are explained by Gilli and Gilli [11-16] and coworkers who described and gave the new name of the new class of the hydrogen bonds in the series of β-diketones. This name: Resonance-assisted hydrogen bond (RAHB) operates in the scientific environment, and is used when we talk about strong or very strong hydrogen bonds with the neutral donor and acceptor which are connected by a system of the π-conjugated double bonds. Due to the fact that the β-diketones are important reagents in the organic synthesis, and have very interesting properties, they have been recently the subject of many experimental and theoretical studies [17-22]. Special attention has been paid to the keto-enol tautomerism of the β-diketones, the structural properties of both keto and enol forms and the nature of the strong O-H…O hydrogen bond in the enol form [23].

Currently in the literature lasts a debate on the matters of shape of the potential well for the β-diketones, especially in the context of the occurrence of the enol forms of β-diketones and the related intramolecular enol-enol forms. In this regard, the scientific community is divided into two groups. Some researchers opt for a well with a single minimum [24-26] and the other claim that it is the well with a double minimum function [27, 28]. In addition, large differences in the shape of the free energy function have been observed for the same substances present in the different states of matter [23-25, 29]. Previous theoretical studies mainly on the DFT level on the benzoylacetone molecule in vacuum found the potential for proton transfer to be a double minimum with a barrier height of ca. 2 kcal/mol [30, 23]. After addition of the zero-point vibrational energy to the total potential energy the internal barrier vanished and effective potential for the proton motion is a single one [30].

In the present article we have described the structures, proton motion, the two-dimensional free-energy landscapes and also the shapes of the O-H…O potential function in the benzoylacetone **(BA) (I)** and dideuterobenzoylacetone **(II) (D_2BA)** in the solid state. Neutron diffraction data shows that in the solid state the enol structure of benzoylacetone with an almost symmetrical enol ring has been found [24, 25]. We have also discussed the isotope effect influence on the shape of the free-energy function by analyzing the results of deuterium substitution obtained from MD simulations. To perform these tasks we used the PIMD method [31, 32] which takes into account the quantum nature of the proton and in consequence it enables to describe a movement of the proton tunneling over the potential barrier thoroughly.

2. Computational details

2.1. Static calculations

A series of full geometry and cell optimizations with the London-type empirical correction for dispersion interactions as proposed by Grimme [33], together with the vibrational harmonic frequency calculations, were undertaken to localize the key stationary points on the potential energy surface (PES) of the 1-phenyl-1,3-butadione (benzoylacetone) (**I**) in the solid state. For the crystal the structural data was taken from the Neutron Diffraction study by Madsen and co-workers [24, 25]. Calculations were performed using the CRYSTAL09 program [34, 35], utilizing the DFT method with PBE functional [36] with the two shrinking factors (7, 7) to generate a commensurate grid of k-points in reciprocal space, following Monkhorst-Pack method [37]. Calculations were carried out with the consistent Gaussian basis sets of triple-zeta valence with polarization quality for solid-state calculations (pob_TZVP_2012) as proposed by Peintinger, Vilela Oliveira, and Bredow [38]. For the both crystals: 1-phenyl-1,3-butadione (benzoylacetone) (**I**) **(BA)** and 1-deuteroxy-2-deutero-1-phenylbut-1-en-3-one (dideuterobenzoylacetone) (**II**) **(D_2BA)** vibrational frequencies calculation in CRYSTAL09 was performed at the Γ-point [34,35].

2.2. Dynamic and quantum dynamic simulations

Molecular dynamics calculations were carried out using the CPMD program version 3.15.3 [39]. The initial molecular configuration for the 1-phenyl-1,3-butadione and 1-deuteroxy-2-deutero-1-phenylbut-1-en-3-one crystals was optimized by the preconditioned conjugate gradient (PCG) method with the London-type empirical correction for dispersion interactions as proposed by Grimme [33] also with Periodic Boundary Conditions (PBCs) was employed for the solid state calculations. In these cases, real space Ewald summation of electrostatic interactions was carried out taking into account 8 cell replicas in each direction. We also generated the Monkhorst-Pack mesh (3,3,3) for calculated k-points in reciprocal space in each direction. The crystals data from the neutron diffraction study by Madsen et al. [24, 25] were selected as starting points. The crystals are monoclinic, benzoylacetone ($P2_1/c$) with cell dimensions a = 8.028, b = 5.483, c = 19.478 Å, and $\alpha = \gamma = 90°$, β = 110.42° with four formula units in the unit cell (Z=4) and dideuterobenzoylacetone ($P2_1/c$) with cell dimensions a = 8.015, b = 5.485, c = 19.462 Å, and $\alpha = \gamma = 90°$, β = 110.34° with four formula units in the

unit cell (Z=4). Molecular dynamics (NVT ensemble) were carried out at 160 K and 300 K respectively with a time step of 3.0 a.u. (0.072566 fs), coupled to a Nosé-Hoover chains thermostat [40] at a frequency of 3200 cm^{-1}. The experimental values of unit cell parameters were used in the CPMD and PIMD simulations. An electronic mass parameter of 600 a.u. was employed. Electronic exchange and correlation have been modeled using the gradient-corrected functional of Perdew, Burke and Ernzerhof (PBE) [36]. Core electrons were treated using the norm-conserving atomic pseudopotentials (PP) of Troullier and Martins [41], while valence electrons were represented in a plane-wave basis set truncated at an extended energy cut-off of 80 Ry. Following the initial equilibration period, data was accrued for further 55 ps for crystals **(I)** and **(II)** Car-Parrinello at two different levels of temperature and for the both crystals imaginary-time (55 ps) for the path integral dynamics simulation, carried out only at 300 K, respectively for eight (PI8) Trotter replicas (polymer-beads) using the normal mode variable transformation. The data was visualized using the VMD [42] and Gnuplot [43] programs; with the path integral data first processed using a script by Kohlmeyer to calculate the centroid position of each set of polymer-beads [44].

The vibrational spectrum was also calculated using the Fourier transformation of the dipole autocorrelation function obtained from dipole trajectories generated by the CPMD simulation facilitated by the scripts of Forbert and Kohlmeyer [45]. It is important to point out that this approach includes anharmonic effects and all of the vibrational modes for molecules in crystals. The lattice vibrations were not received because fixed experimental values of unit cell were used.

3. Results and discussion

3.1. Structure analysis

The molecular geometry (in the unit cell) and atoms labeling of 1-phenyl-1,3-butadione (benzoylacetone, **BA**) in the solid state and its deuterated analogue are shown in Figure 1. The red labeling was used for the second structure when two hydrogen atoms (H1, H5) in a single molecule has been substituted by deuterium. In the Table 1 the calculated selected interatomic distances and angles after optimization compared with the average geometrical parameters from CPMD (standard deviation in brackets) and with the existing experimental data for both crystals are presented. As can be inferred from Table 1, distances between heavy atoms in the hydrogen bond (O1-O2) in the studied crystals are very short (ca. 2.5 Å) and have a similar

length regardless of the method of analysis. We can also notice that the average lengths of the deuterated bridge in the analogue **(II)** are slightly longer than the average lengths of the H-bridge of the structure **(I)**. It shows very good agreement of computed MD geometrical parameters with the neutron diffraction experiment [24, 25]. However, the geometry optimization on the static methods level slightly underestimates the length of the hydrogen bridge, about 0.051 Å for the structure **(I)**. Analyzing the geometric structure of the molecule in terms of the prevalence of characteristics model RAHB, we should carefully look at the length of the four bonds in the keto-enol parts of the molecule. Taking to the analysis our simulations carried out on the static and especially on dynamic levels, we can be conclude that the bond lengths (O1=C2/O2-C4 and C4=C3/C2-C3) coincide with the typical lengths for the bonds determined experimentally. For example, let us analyze the data from the both simulations for the crystal **(I)**, static optimization on the DFT method level and molecular dynamics in terms of Car-Parrinello. The resulting values are presented in order O1=C2/O2-C4 (1.286/1.336 Å) and C4=C3/C2-C3 (1.388/1.418 Å); O1=C2/O2-C4 (1.290/1.316 Å) and C4=C3/C2-C3 (1.406/1.415 Å) for DFT and CPMD methods respectively. It can be concluded that the equivalence of the bond lengths may be attributed to delocalization over a conjugated the π-bonded system in the keto-enol group [15]. Quoted values of the bonds lenght clearly indicates a different chemical bonds character. These bonds O2-C4, C2-C3 are single and O1=C2, C4=C3 have double character. Additionally, we have a relatively short hydrogen bridge and not ideal symmetrical position of the proton. All of these features fit well in the assumptions of the model RAHB proposed by Gilly [15]. Noteworthy is the fact a large non-linearity of the hydrogen bond. Each of the methods of calculation indicates that the angles values of the hydrogen bridge are between 150 and 157 degrees, which are close to the experimental [24, 25] data. We would like also to draw attention to the good agreement of computational results with the experimental data of the dihedral angles, as it is shown in the Table 1. In our opinion this confirms the correctness of the implementation of the simulation, since these parameters are particularly sensitive to structural errors [46]. Moreover, the optimized parameters of the unit cell are in reasonable agreement with experimental values [24, 25]. The largest error (ca. 10%) is noted for *a* parameter. For remaining lattice parameters errors between optimized and experimental values are smaller than 5%. It seems to confirm the need to use dispersion corrections to the full energy at calculations on the DFT method level [47].

3.2. Molecular dynamics simulations

The CP dynamic simulations were performed at two different temperatures because the experimental data for crystals are reported in this manner [26], while PIMD simulations were conducted only at 300 K due to a very high computational cost. The time evolution behavior of the bond lengths directly involved in the selected intramolecular hydrogen bonds O2-H1(D1)…O1 from crystal **(I)** and **(II)** at 160 K and 300 K is presented in Figure 2. Careful analysis of the strong O2-H1(D1)...O1 intramolecular hydrogen bond shows very large fluctuation of the bridging proton/deuter between the two oxygen atoms in crystal **(I)** and **(II)** at 160 K (see Fig. 2a, 2c) and much larger mobility of proton/deuter in hydrogen bridge in the simulations at 300 K (see Fig. 2b, 2d). As we expected higher temperature of simulation causes more frequent proton/deuter hops (transfer). At the temperature of 160 K proton/deuter jumps about 80 times while in the 300 K almost three times more often. According to our estimates, the full process of proton hopping in the crystal of benzoylacetone takes about 12-16 fs, which is close to the experimental and theoretical data [5, 6]. When we analyze the results of the PIMD simulation, when the quantum effects are taken into account, it can be seen that the proton/deuter is completely delocalized between two carbonyl oxygens (see Fig. 3). From the CPMD simulations at 160 K the O2-H1(D1) bonds length changes in the ranges 0.953 - 1.895 Å for the crystal (**I)** and 0.896 - 2.052 Å for the crystal (**II)**, while at 300 K the O2-H1(D1) bonds length changes in the ranges 0.945 - 1.887 Å for the crystal (**I)** and 0.917 - 2.108 Å for the crystal **(II)**. Averaged O2-H1(D1) distances from the Molecular dynamics method (see Tab. 1) are strong dependent on temperature and their values are 1.164/1.161 Å and 1.225/1.205 Å for the crystal **(I)** and **(II)** at 160 and 300 K, respectively. Following the distance of the hydrogen bridge, we observe that the O-H bonds are extremely sensitive to changes of temperatures. This phenomenon has been described by Wilson and co-workers [50] on base of single neutron diffraction studies for the benzoic acid crystal. The analysis of the distribution function of proton/deuter in the hydrogen bridge shows importance of quantum effects. Their inclusion in the calculation completely changes the picture of physical processes. Please look at the Figures 4 and 5 where we have presented the distribution functions (δ-parameter) of proton/deuter position along the reaction coordinate on the base of our results from the CPMD and PIMD method. In order to show the influence of quantum effects better, we have prepared a series of graphs of free energy. Figures 6 and 7 shows the free energy profiles for proton motion obtained from the CPMD and PIMD results. Free energy profiles were calculated following the equation:

$$\Delta F = -kT \ln[P(\delta)], \quad (1)$$

where k is the Boltzmann constant, T is the simulation temperature, and P(δ) is the proton distribution as a function of δ (the reaction coordinate), which is defined as the difference between distances $r_{O\text{-}H(D)} - r_{H(D)\text{-}O}$ and is a measure of the proton/deuter transfer degree in the hydrogen bond. The value of zero indicated the midpoint of the hydrogen/deuter position in H/D-bond. The profiles of the free energy in Figure 6 demonstrate the absence of the effective barrier for proton transfer even without an inclusion of quantum effects for the CPMD simulation. Calculations show that the quantity of the barrier for proton transfer in the crystal of **BA** and its deuterated analogue are about 0.25 kcal/mol and decreases as the temperature increases to about 0.15 kcal/mol. This would suggest that during the process of proton transfer we have observed the potentials wells with a double minimum but the quantum effects taken into account do change the effective potential shape drastically, as it is shown on Figures 7a, 7b. These strong HBs have also been named low-barrier hydrogen bonds (LBHB) [51]. It is interesting to notice that the results of CPMD simulations (the double well potential) are very similar to the static DFT calculations of **BA** molecule in vacuum [30, 23] whereas the CPMD simulations are in very good accord with experimental observation showing almost symmetrical H-bond [24, 25].

In order to deeper analysis of the proton mobility in studied intramolecular H-bonds we constructed two-dimensional free-energy landscapes from two-dimensional distribution of δ-parameter and O…O distances, illustrated in Figures 8, 1S, 2S and 3S (in supplementary materials), for every hydrogen bridge in the crystal unit, for further analysis on the proton/deuter transfer. As shown in the series of figures from 8 to 3S, the fragments (a) and (b) presented the free energy surfaces obtained for crystal **(I)** from CPMD simulations and fragment (c) from PIMD simulations. Similarly, the section (d), (e) and (f) of Figures were obtained for the second crystal **(II)**. Let us now carry out a brief discussion of the above-mentioned landscapes. As shown sections (a, b, d and e) of Figures, the free energy surfaces obtained from CP simulations have two minima, while sections (c) and (f) obtained from PIMD simulations have one minimum, in each case. As it has been shown in Figures 7a and 7b the nuclear quantum effects remove the proton transfer barrier allowing barrier-less proton transfer. Looking at the two-dimensional free-energy landscapes we can also see a substantial mobility and relocation of the proton position at higher temperatures of simulations and

negligible impact of isotope effect on the shape and height of the energy barrier of proton/deuter transfer. Moreover, despite the fact that the potential well has one minimum, the position of the proton/deuter is not perfectly symmetrical. It is a very subtle effect, which is often accompanied by typical resonance assisted hydrogen bond.

According to Gilli and Gilli [15, 16], for the description resonance-assisted hydrogen bonded systems, very important is so-called π-delocalization index defined as:

$$\Lambda = \frac{1}{2}\left(1 - \frac{Q}{0.32}\right), \qquad (2)$$

where the $Q = (d_1 - d_4) + (d_3 - d_2)$. In our studies the delocalization parameters (Q) for **BA** crystal and its deuterated analogue were described by relevant molecular distances Q = (O2-C4 – O1-C2) + (C2-C3 – C3-C4). According to Gilli and co-workers [15], Q = 0 corresponds to the fully π-delocalized structure and Q = -0.32 or +0.32 Å to the completely localized bonding. The Λ value of 0.5 indicates to a fully delocalized keto-enolic system whereas Λ value closer to 0 or 1 indicates localized bonding. Two-dimensional plot of delocalization parameter Q versus $R_{O1\ldots O2}$ distance for crystals **(I)** and **(II)** are shown in Figure 9. Values of Λ and Q are calculated on the base of the average bond lengths from CPMD simulation. In both cases, the Λ-parameter is equal 0.445. After a precise analysis of Figure 9 we can conclude that the intramolecular hydrogen bond in the crystal of **BA** can be classified into the group of hydrogen bond with RAHB character. In addition, Figure 9 allows observing the correlation between the Q and Λ parameters and the length of the hydrogen/deuter bridge throughout the course of the simulation. Therefore, according to the classification proposed by Gilli and co-workers [15], it can be concluded that changes in the hydrogen bonds and other bonds coupled with the molecular system are characterized by the type of strong π-delocalized structure (enol-enol forms). However, it should be noticed, that in this disordered molecular system there are two forms with a slightly more contribution of the π-localized enol-keto (EK) form than π-localized keto-enol (KE) form. We think that these results mainly from a little asymmetrical position of the proton/deuter in the bridge.

Calculated and experimental value of the O1…O2 distance close to 2.5 Å might suggest strong O-H…O intramolecular bond. Estimation of the strength of intramolecular H-bonds for systems in a crystal is not trivial. One of the simplest methods of determination H-bond strength in vacuum is the calculation of the difference in energy between closed (X-H…Y) and open configuration. However, this approach can not be applied for a system in a crystal.

Therefore, for the estimation of this intramolecular H-bond we have used the very simple relation proposed by Musim and Marian [52]:

$$E_{HB} = (5.554 \times 10^5) \exp(-4.12R) \quad (3)$$

where R is the O…O distance. Using the value of 2.5 Å which is close to the experimental and average values from CPMD simulations the estimated H-bond strength is equal to -18.7 kcal/mol. The strength of H-bond in a crystal estimated by us is in good agreement with the value of -16.3 kcal/mol obtained in vacuum on base of DFT calculations by Schiøtt and coworkers [30]. It means that this H-bond is strong in the group of intramolecular hydrogen bonds.

3.3. IR spectra

Selected characteristics of vibrational frequencies from CPMD, together with harmonic frequencies from static calculations and available experimental data, are presented in Table 2 for crystal **(I)** and **(II)** respectively. Figure 10 presents the CPMD infrared spectrum for both examined crystals **BA** and **D_2BA** with experimental spectra for **BA** crystal [53, 54]. We also constructed the comparison of simulated and experimental spectra for **BA** crystal and its deuterated analogue, illustrated in Figure 11, for further comparative vibrational analysis. The assignments of the calculated frequencies are based on the experimental IR [53] spectra for benzoylacetone and its deuterated analogue. As we know, the infrared spectroscopy is one of very useful experimental methods for studies on the strength of the hydrogen bond and it is also very important since it proves that the results of molecular dynamics simulation are correct. In the context of this paper, seems to be the most important the analysis of the vibration frequency of –OH groups. The characteristics of –OH stretching vibration in the enol form of the β-diketones appears as a weak and very broad band at the 3300-2000 cm^{-1} region [55-58]. The intensity and broadness of this band are depended on the strength of the intramolecular hydrogen bond [53]. We have observed that the stretching vibrations –OH/–OD are shifted in comparison to the –OH/–OD frequencies of bonds not involved in H-bond to lower frequencies about 2217/1681 cm^{-1} and 2514/1922 cm^{-1} for crystal **(I)** and **(II),** respectively, in both calculation methods. The calculated stretching vibrations –OH/–OD are in good agreement with experimental results (2650/1960 cm^{-1}) but it seems that the CP molecular dynamics method reproduces frequencies of vibrations better than static methods in

harmonic approximation in every case. As compared with the experiment, most of the frequencies from CPMD methods are slightly shifted toward a lower frequency, however, no clear tendency can be observed because some frequencies are a little bit higher. As we expected we have observed the very large red shift effects of –OH stretching vibrations in these molecular systems. This phenomenon is typical for the incidence of enol-enol resonance structure with the strong intramolecular hydrogen bond.

Very important parameter related with the IR spectra of H-bonded systems is the isotope effect, defined by the isotopic ratio (ISR) νOH/νOD. Due to the anharmonicity in majority of H-bonded systems, the ISR value is different from √2. It has been shown that in the case of O-H…O H-bonds, the maximum value of ISR does not exceed 1.5 [59]. The calculated ISR values equal 1.32, 1.31, 1.35 from the static calculations, CPMD simulations and experiment, respectively. These values also indicate a very strong hydrogen bond and high mobility of the proton in the hydrogen bridge. Noteworthy is also the fact that we have observed a good agreement the experimental data (3110/2313 cm^{-1}) with the calculated (3186/2361 cm^{-1} and 3107/2336 cm^{-1}) values for –CH/–CD stretching vibration frequency. In this case we can also see a very large isotopic effect for these vibrations. The O…O stretching mode for **BA** in the experiment appears at about 396/384 cm^{-1}. According to our static and CP calculations these modes are located at about 410/395 cm^{-1} and 345/279 cm^{-1}, respectively. The ν O…O mode is coupled with δ C-CH_3 and the position of this band relates to the other β-diketones which also suggests the incidence of very strong HB.

4. Conclusion

We have presented the results of theoretical studies on the intramolecular hydrogen bonds in 1-phenyl-1,3-butadione and its deuterated analogue 1-deuteroxy-2-deutero-1-phenylbut-1-en-3-one in the solid state using static as well as *ab initio* molecular dynamics methods. In our study of both crystals we have found evidence for existing strong π-delocalized structure (enol-enol forms) with location of the enol hydrogen in a very flat slightly asymmetric (almost symmetry) single minimum potential, which is in accordance with neutron diffraction studies performing by Madsen [24, 25] and coworkers. The analysis of the average distances in the geometric structure of the four bonds in the keto-enol parts of the molecule indicated that the equivalence of the bond lengths may be attributed to delocalization over a conjugated π-bonded system in the keto-enol group. We also calculated the π-delocalization index for both crystals taking as the basis for calculating the average bond lengths from CPMD simulation is

equal 0.445. In addition, the calculated correlation between the Q and the Λ parameters and the length of the hydrogen/deuter bridge throughout the course of the simulation shows that the system is characterized by the type of strong π-delocalized structure (enol-enol forms) with slightly more contribution of the π-localized enol-keto (EK) form than π-localized keto-enol (KE) form. In our opinion, all the arguments given above (a relatively short hydrogen bridge, the not ideal symmetrical position of the proton, the shape of the potential function of proton, the correlation between the Q and the Λ parameters and a very big red shift effects of –OH stretching vibrations) indicate that the hydrogen bond in the benzoylacetone crystals have properties characteristic for the type of bonding model resonance assisted hydrogen bonds without existing equilibrium of the two tautomers.

Author information

Corresponding author

* Email: piotr@elrond.chem.uni.wroc.pl

Website: http://kwanty.wchuwr.pl/?q=durlak

Acknowledgement

This paper is dedicated to the memory of my wonderful Mother, who recently passed away. The authors would like to gratefully acknowledge the Academic Computer Centre in Gdansk (CI TASK) for the use of the Galera-ACTION Cluster and the Wroclaw Centre for Networking and Supercomputing (WCSS) for the use of the Supernova Cluster. Dr. Przemysław Dopieralski is acknowledged for helpful discussion as well as help with preparing the AWK's scripts.

Supplementary materials

On Figures 1S – 3S are presented two-dimensional free-energy landscape of δ-parameter (reaction coordinate) $R_{O3...O4}$, $R_{O5...O6}$, and $R_{O7...O8}$ distances, respectively, for crystal **(I)** and crystal **(II)**. This material is available free of charge via the Internet at http://.....

References

1 T. Steiner, *Angew. Chem. Int. Ed.*, 2002, **41**, 48.

2 G. A. Jeffrey in *An Introduction of Hydrogen Bonding*, Oxford University Press: New York, USA, 1997.

3 W. W. Cleland, M. M. Kreevoy, *Science*, 1994, **264**, 1887.

4 A. Warshel, A. Papazyan, P. A. Kollman, *Science*, 1995, **269**, 102.

5 G. R. Desiraju, T. Steiner in *The Weak Hydrogen Bond: In Structural Chemistry and Biology.(International Union of Crystallography Monographs on Crystallography; no. 23)*, Oxford University Press, USA, 1997.

6 P. Durlak, K. Mierzwicki, Z. Latajka, *J. Phys. Chem. B*, 2013, **117**, 5430.

7 P. Sanz, O. Mó, M. Yáñez, J. Elguero, *J. Phys. Chem. A*, 2007, **111**, 3585.

8 R. N. Singh, A. Kumar, R. K. Tiwari, P. Rawat, V. Baboo, D. Verma, *Spectrochim. Acta A*, 2012, **92**, 295.

9 H. Karabıyık, R. Sevinçek, H. Petek, M. Aygün, *J. Mol. Model*., 2012, **17**, 1295.

10 S. W. Rick, S. J. Stuart in *Potentials and Algorithms for Incorporating Polarizability in Computer Simulations.*, ed. K. B. Lipkowitz, T. R. Cundari, V. J. Gillet, D. B. Boyd, vol. 18, in *Reviews in Computational Chemistry*, Wiley-VCH: Hoboken, New Jersey, 2002; pp. 89–146.

11 P. Gilli, V. Bertolasi, L. Pretto, L. Antonov, G. Gilli, *J. Am. Chem. Soc.*, 2005, **127***,* 4943.

12 P. Gilli, V. Bertolasi, L. Pretto, V. Ferretti, G. Gilli, *J. Am. Chem. Soc.*, 2004, **126**, 3845.

13 P. Gilli, V. Bertolasi, V. Ferretti, G. Gilli, *J. Am. Chem. Soc.*, 1994, **116**, 909.

14 V. Bertolasi, P. Gilli, V. Ferretti, G. Gilli, *J. Am. Chem. Soc.*, 1991, **113***,* 4917.

15 G. Gilli, F. Bellucci, V. Ferretti, V. Bertolasi, *J. Am. Chem. Soc.*, 1989, **111**, 1023.

16 G. Gilli, P. Gilli in *The Nature of the Hydrogen Bond: Outline of a Comprehensive Hydrogen Bond Theory (International Union of Crystallography Monographs on Crystallography; no. 23)*, Oxford University Press, USA, 2009.

17 N. V. Belova, V. V. Sliznev, H. Oberhammer, G. V. Girichev, *J. Mol. Struct.*, 2010, **978**, 282.

18 F. Gomez-Garibay, J. S. Calderon, L. Quijano, O. Tellez, M. Soccoro-Olivares, T. Rios, *Phytochemistry*, 2001, **46**, 1285.

19 F. Wetz, C. Routaboul, D. Lavabre, J. C. Garrigues, I. Rico-Latters, I. Pernet, A. Denis, *Photochem. Photobiol.*, 2004, **80**, 316.

20 V. Bertolasi, V. Ferretti, P. Gilli, X. Yao, Ch. –J Li, *New J. Chem.*, 2008, **32**, 694.

21 C. M. Silvernail, G. Yap, R. D. Sommer, A. L. Rheingold, V. W. Day, J. A. Belot, *Polyhedron*, 2001, **20**, 3113.

22 J. A. Belot, J. Clark, J. A. Cowan, G. S. Harbison, A. I. Kolesnikov, Y. –S. Kye, A. J. Schultz, C. Silvernail, X. Zhao, *J. Phys. Chem. B*, 2004, **108**, 6922.

23 N. V. Belova, G. V. Girichev, H. Oberhammer, T. N. Hoang, S. A. Shlykov, *J. Phys. Chem. A*, 2012, **116**, 3428.

24 G. K. H. Madsen, B. B. Iversen, F. K. Larsen, M. Kapon, G. M. Reisner, F. H. Herbstein, *J. Am. Chem. Soc.*, 1998, **120**, 10040.

25 G. K. H. Madsen, G. J. McIntyre, B. Schiøtt, F. K. Larsen, *Chem. Eur. J.*, 2007, **13**, 5539.

26 F. H. Herbstein, B. B. Iversen, M. Kapon, F. K. Larsen, G. K. H. Madsen, G. M. Reisner, *Acta Cryst. B*, 1999, **55**, 767.

27 S. I. Chan, L. Lin, D. Clutter, P. Dea, *Proc. Natl. Acad. Sci. USA*, 1970, **65**, 816.

28 E. V. Borisov, E. V. Skorodumov, V. M. Pachevskaya, P. E. Hansen, *Magn. Reson. Chem.*, 2005, **43**, 992.

29 J. W. Bunting, J. P. Kanter, R. Nelander, Z. Wu, *Can. J. Chem.*, 1995, **73**, 1305.

30 B. Schiøtt, B. B. Iversen, G. K. H. Madsen, T. C. Bruice, *J. Am. Chem. Soc*., 1998, **120**, 12117.

31 D. Marx in Advanced Car-Parrinello Techniques: Path Integrals and Nonadiabaticity In Condensed Matter Simulations, ed. M. Ferrario, G. Ciccotti, K. Binder, vol. 704, in *Computer Simulations in Condensed Matter Systems: From Materials to Chemical Biology Volume 2, Lect. Notes Phys.*, Springer: Berlin, 2006, pp. 507–539.

32 M. E. Tuckerman in Path Integration via Molecular Dynamics., ed. J. Grotendorst, D. Marx, A. Muramatsu, vol. 10 in *Quantum Simulation of Complex Many-Body Systems: From Theory to Algorithms*, John von Neumann Instituite for Computing (NIC): Juelich, Germany, 2002, pp. 269–298.

33 S. J. Grimme, *J. Comput. Chem.*, 2006, **27**, 1787.

34 CRYSTAL09 User's Manual, University of Torino; R. Dovesi, V. R. Saunders, C. Roetti, R. Orlando, C. M. Zicovich-Wilson, F. Pascale, B. Civalleri, K. Doll, N. M. Harrison, I. J. Bush, Ph. D'Arco, M. Llunell, Torino, 2009.

35 R. Dovesi, R. Orlando, B. Civalleri, C. Roetti, V. R. Saunders, C. M. Zicovich-Wilson, *Z. Kristallogr.*, 2005, **220**, 571.

36 J. P. Perdew, K. Burke, M. Ernzerhof, *Phys. Rev. Lett.*, 1996, **77**, 3865.

37 H. J. Monkhorst, J. D. Pack, *Phys. Rev.B*, 1976, **13**, 5188.

38 M. F. Peintinger, D. Vilela Oliveira, T. Bredow, *J. Comput. Chem.*, 2013, **34**, 451.

39 CPMD, version 3.15.3; Copyright IBM Corp 1990-2008, Copyright MPI für Festkörperforschung Stuttgart 1997-2001; http://www.cpmd.org.

40 G. J. Martyna, M. L. Klein, M. Tuckerman, *J. Chem. Phys.*, 1992, **97**, 2635.

41 N. Troullier, J. L. Martins, *Phys. Rev. B*, 1991, **43**, 1993.

42 W. Humphrey, A. Dalke, K. Schulten, *J. Molec. Graphics.*, 1996, **14**, 33.

43 Gnuplot 4.5 (patchlevel 5); Williams, T.; Kelley, C.; http://gnuplot.info.; 2014.

44 traj2xyz.pl, version 1.4.; A. Kohlmeyer, H. Forbert, 2004.

45 Fourier, version 2; H. Forbert, A. Kohlmeyer, 2002-05.

46 P. Durlak, Z. Latajka, *J. Mol. Model.*, 2011, **17**, 2159.

47 P. Durlak, Z. Latajka, *J. Chem. Theory Comput.*, 2013, **9**, 65.

48 C. A. Morrison, M. M. Siddick, P. J. Capm, C. C. Wilson, *J. Am. Chem. Soc.*, 2005, **127**, 4042.

49 S. Pantano, F. Alber, P. J. Carloni, *J. Mol. Struct. Theochem*, 2000, **530**, 177.

50 C. C. Wilson, N. Shankland, A. J. Florence, *Chem. Phys. Lett.*, 1996, **253**, 103.

51 W.W. Cleland, *Biochemistry*, 1992, **31**, 317.

52 R. N. Musin, Y. H. Marian, *J. Phys. Org. Chem.*, 2006, **19**, 425.

53 S. F. Tayyari, J. S. Emampour, M. Vakili, A. R. Nekoei, H. Eshghi, S. Salemi, M. Hassanpour, *J. Mol. Struct.*, 2006, **794**, 204.

54 NIST/EPA Gas-Phase Infrared Database JCAMP Format. http://webbook.nist.gov/cgi/cbook.cgi?ID=C93914&Mask=80#Refs

55 S. F. Tayyari, F. Milani-Nejad, *Spectrochim. Acta A*, 2000**, 56**, 2679.

56 R. R. Lozada-Garcia, J. Ceponkus, W. Chin, M. Chevalier, C. Crépin, *Chem. Phys. Lett.*, 2011, **504**, 142.

57 Z. Yoshida, H. Ogoshi, T. Tokumitsu, *Tetrahedron*, 1970, **26**, 5691.

58 S. F. Tayyari, T. Zeegers-Huyskens, J. L.Wood, *Spectrochim. Acta A*, 1979, **35**, 1265.

59 Z. Latajka, L. Sobczyk in The Potential Energy Shape for the Proton Motion In Protonated Naphthalene Proton Sponges (DMAN-s) and its Manifestations, ed. J. Leszczynski, M. K. Shukla in *Practical Aspects of Computational Chemistry. Methods, Concepts and Applications*, Springer, Heidelberg, Dordrecht, London, New York, 2010, pp. 371–386.

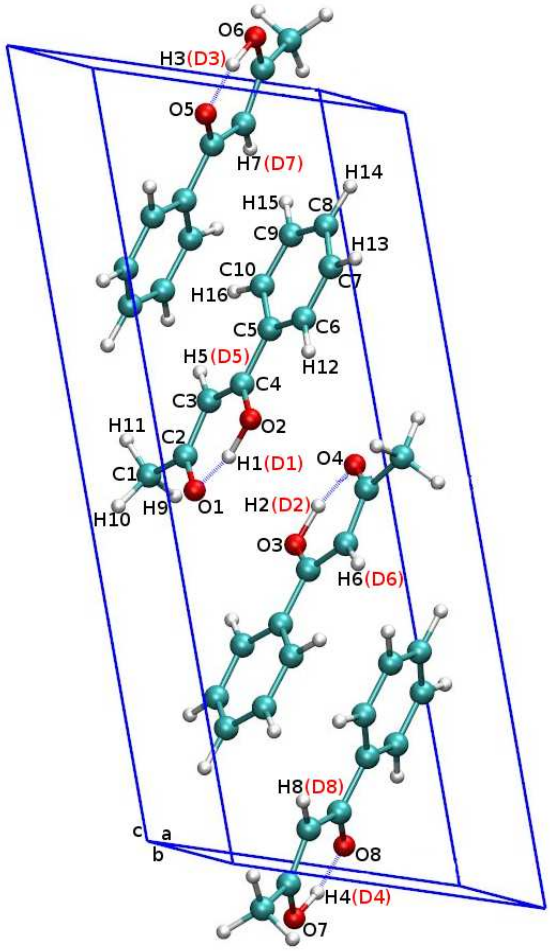

Figure 1. The unit cell and atoms labeling of 1-phenyl-1,3-butadione (benzoylacetone) crystal. The red color of labels is for dideuterobenzoylacetone crystal.

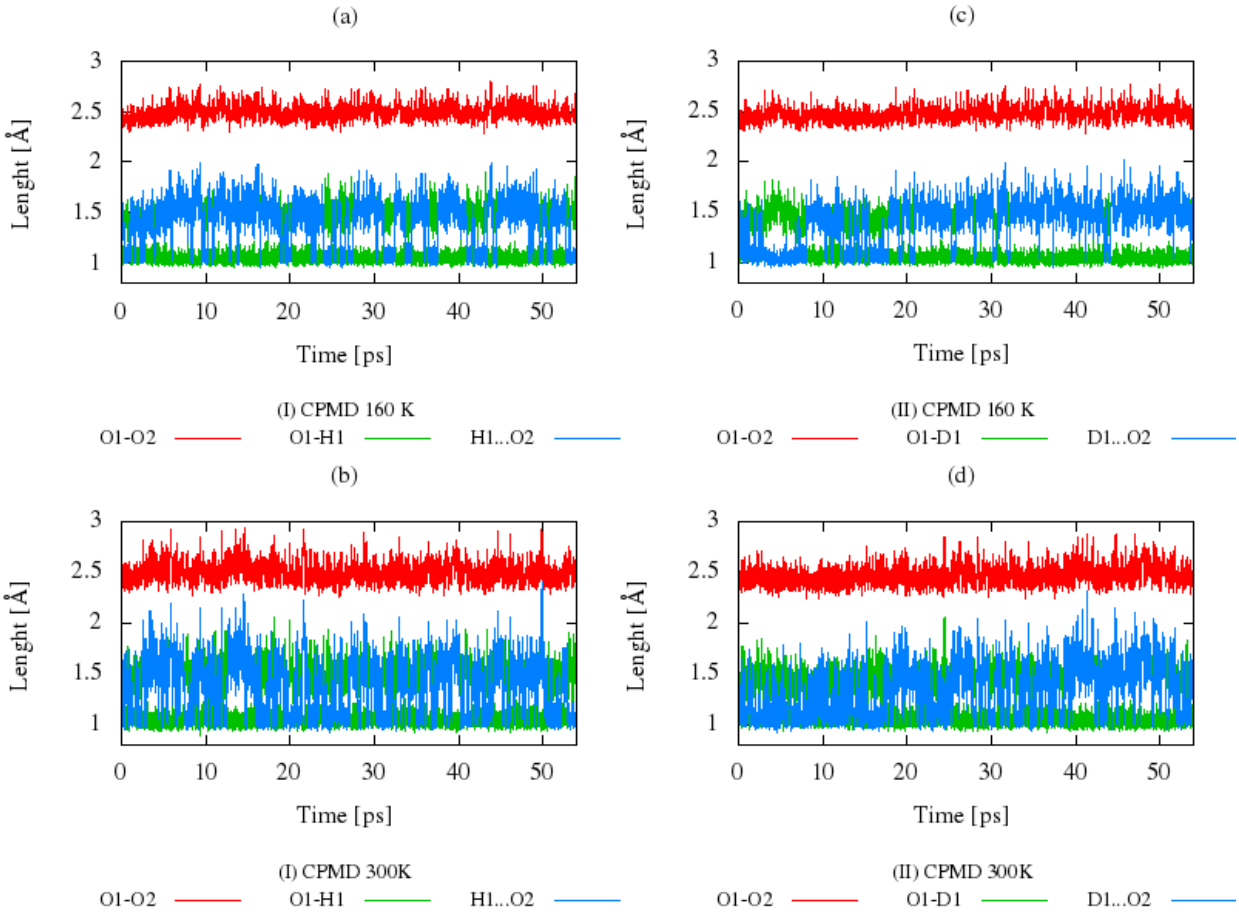

Figure 2. Time evolution of bonds involved in the hydrogen bonds O1-H1(D1)…O2 for (a) benzoylacetone at 160 K, (b) benzoylacetone at 300 K and for (c) dideuterobenzoylacetone at 160K, (d) dideuterobenzoylacetone at 300 K from the CPMD calculations.

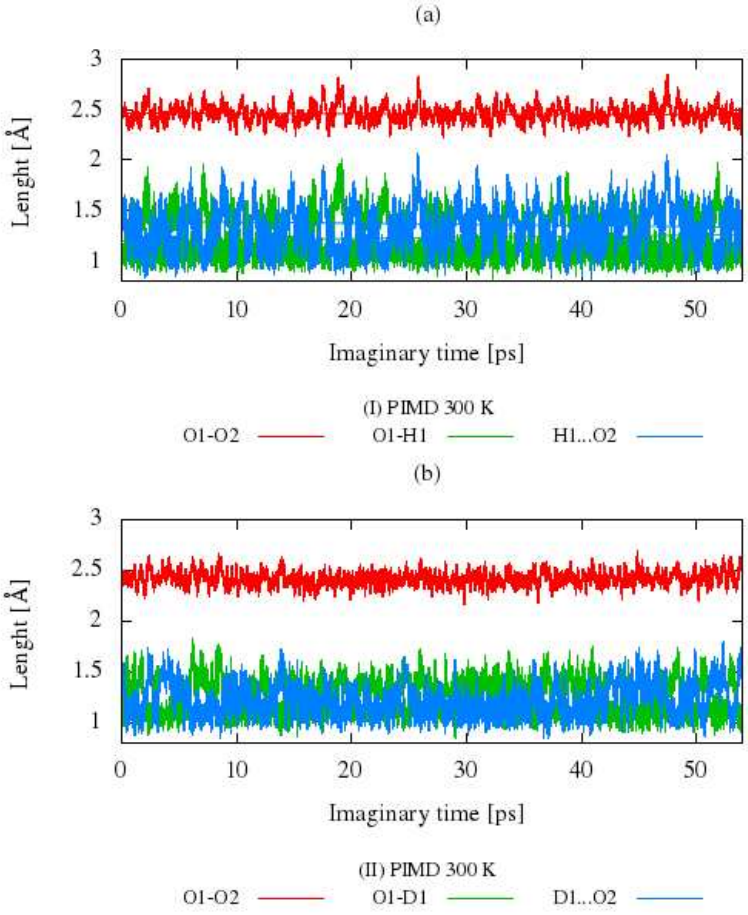

Figure 3. Time evolution of bonds involved in the hydrogen bonds O1-H1(D1)…O2 for (a) benzoylacetone at 300 K and for (b) dideuterobenzoylacetone at 300 K from the PIMD calculations.

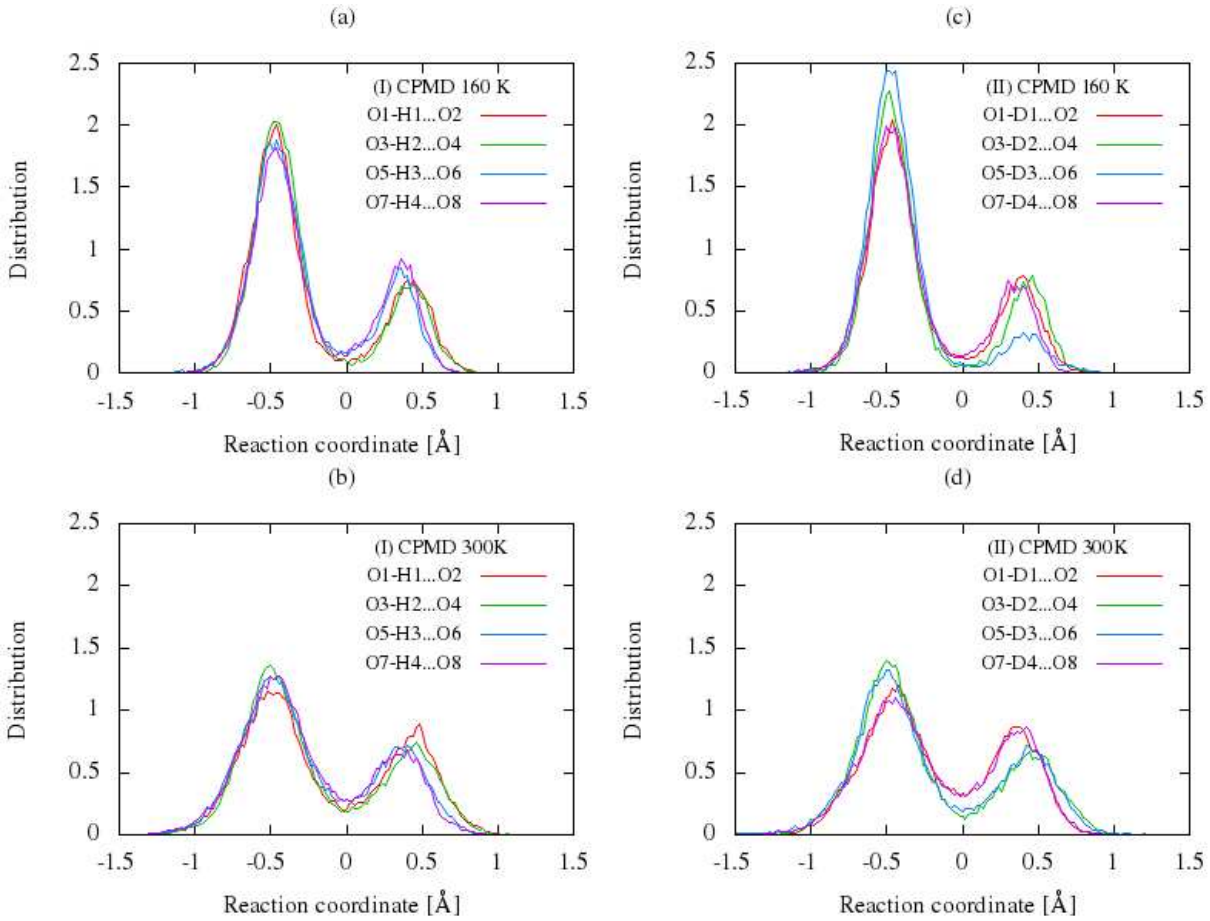

Figure 4. Comparison of the distribution functions (δ-parameter) from CPMD simulations for the intramolecular H-bonds for (a) benzoylacetone at 160 K, (b) benzoylacetone at 300 K and for (c) dideuterobenzoylacetone at 160K, (d) dideuterobenzoylacetone at 300 K.

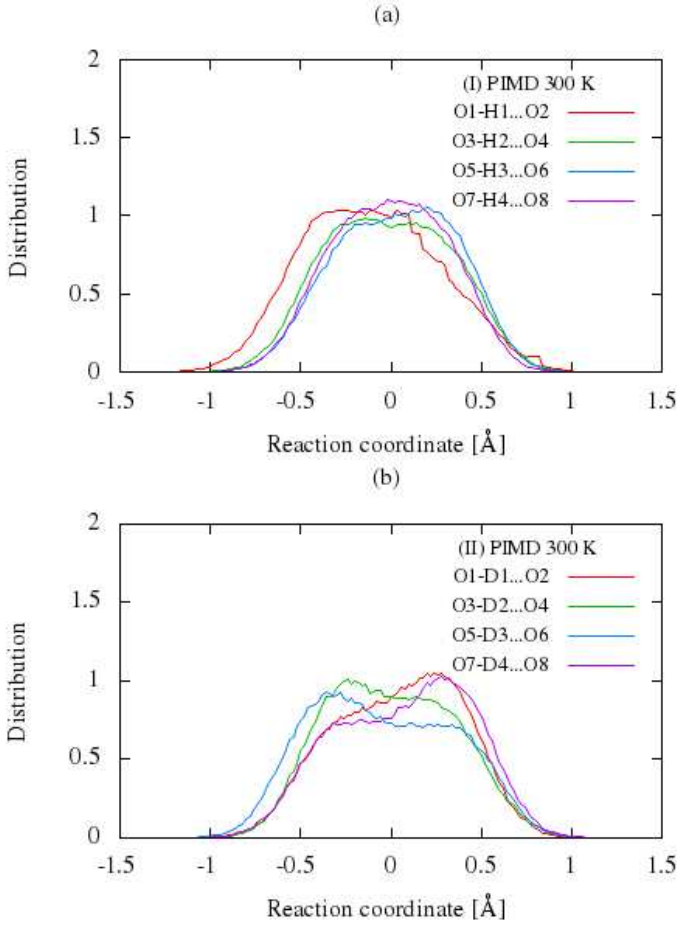

Figure 5. Comparison of the distribution functions (δ-parameter) from PIMD simulations for the intramolecular H-bonds for (a) benzoylacetone at 300 K and (b) dideuterobenzoylacetone at 300 K.

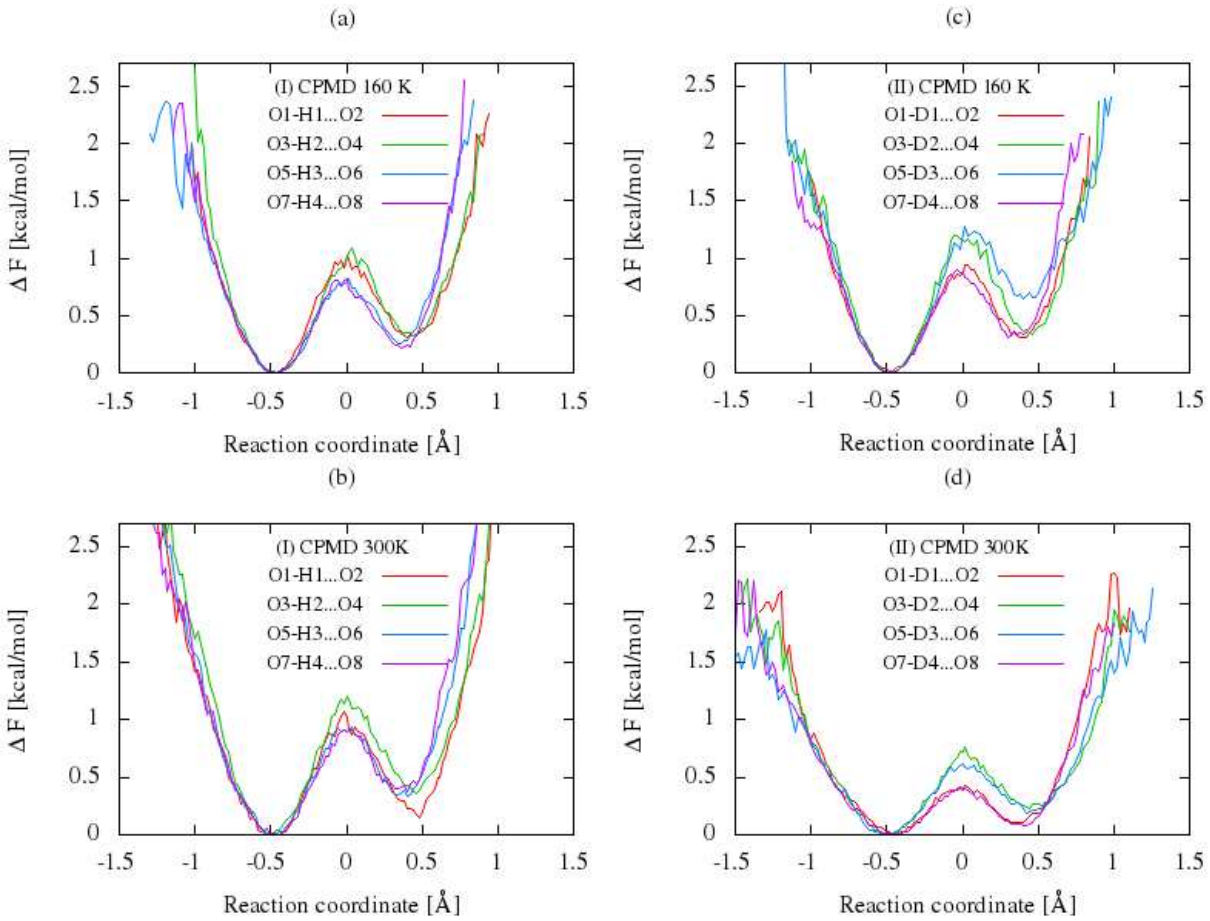

Figure 6. Comparison of the single proton transfers free-energy ΔF profiles from CPMD simulations for the intramolecular H-bonds for (a) benzoylacetone at 160 K, (b) benzoylacetone at 300 and for (c) dideuterobenzoylacetone at 160K, (d) dideuterobenzoylacetone at 300 K.

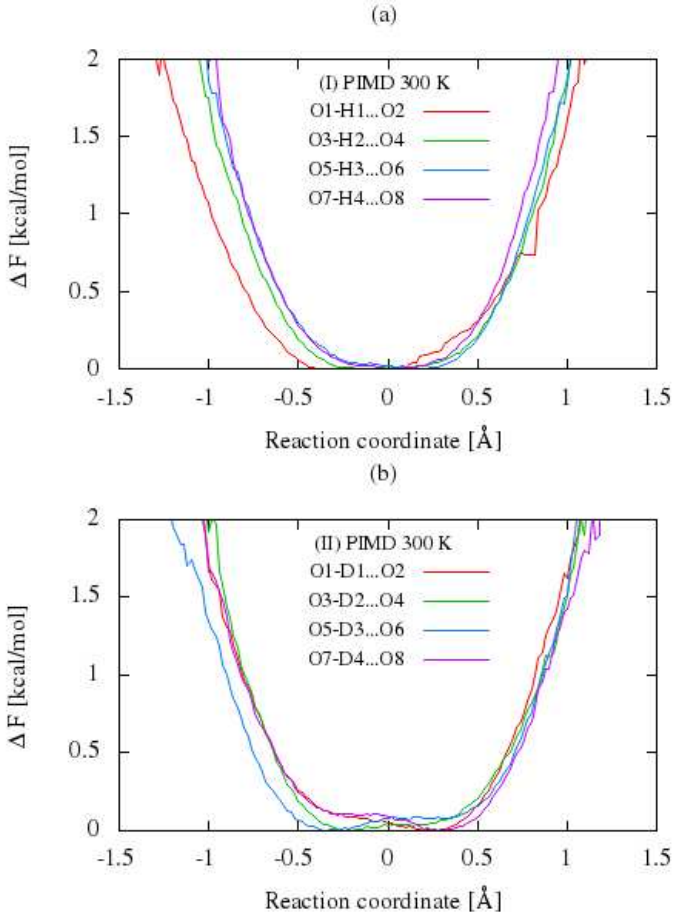

Figure 7. Comparison of the single proton transfers free-energy ΔF profiles from PIMD simulations for the intramolecular H-bonds for (a) benzoylacetone at 300 and for (b) dideuterobenzoylacetone at 300 K.

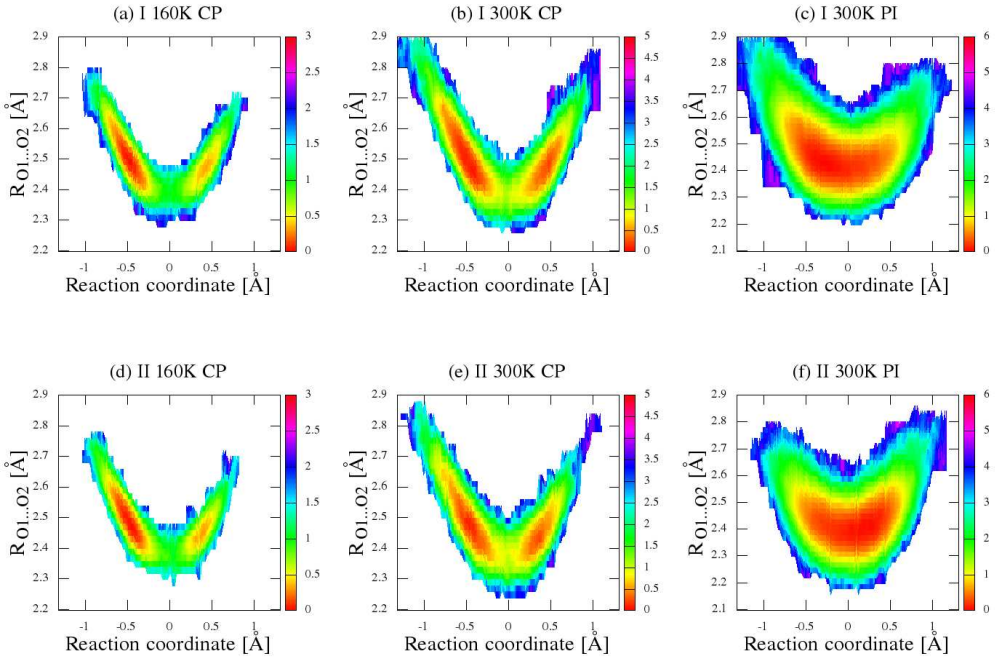

Figure 8. Two-dimensional free-energy landscape of δ-parameter (reaction coordinate) and $R_{O1...O2}$ distances for crystal **(I)** for (a) CPMD simulation at 160 K, (b) CPMD simulation at 300 K, (c) PIMD simulation at 300 K, and for crystal **(II)** for (d) CPMD simulation at 160 K, (e) CPMD simulation at 300 K, (f) PIMD simulation at 300 K. The unit of ΔF free energy (potential of mean force) is kcal/mol.

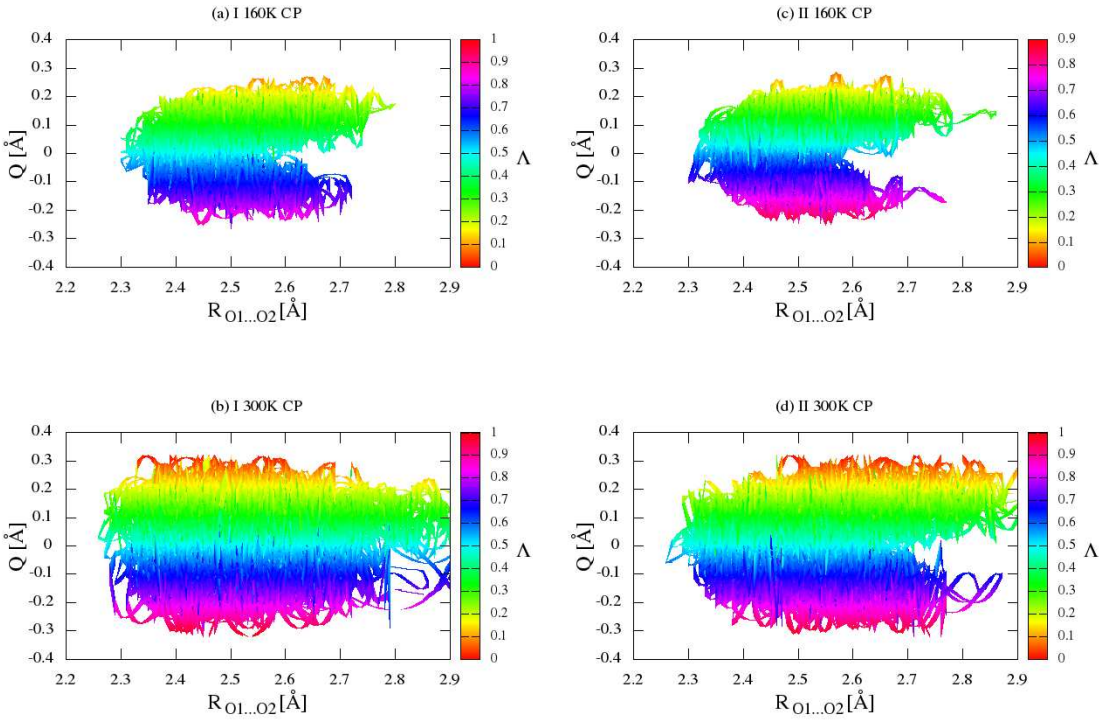

Figure 9. Two-dimensional π-delocalization index (Λ) landscape of $R_{O1...O2}$ distances and delocalization parameter (Q) for crystal **(I)** for (a) CPMD simulation at 160 K, (b) CPMD simulation at 300 K, and for crystal **(II)** for (c) CPMD simulation at 160 K, (d) CPMD simulation at 300 K.

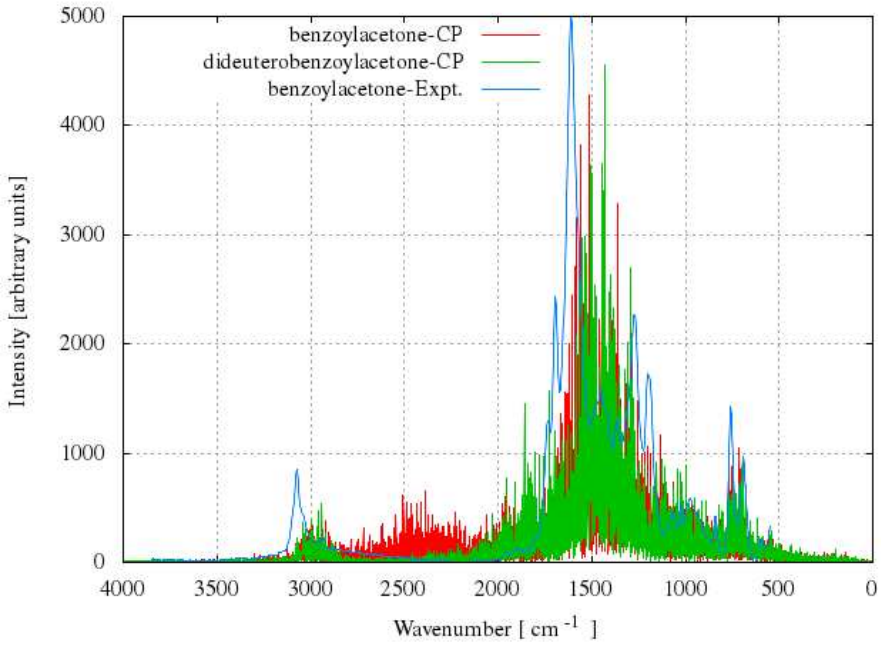

Figure 10. Comparison of the experimental (blue line) [53, 54] and simulated IR spectra for benzoylacetone (red line) and dideuterobenzoylacetone (green line).

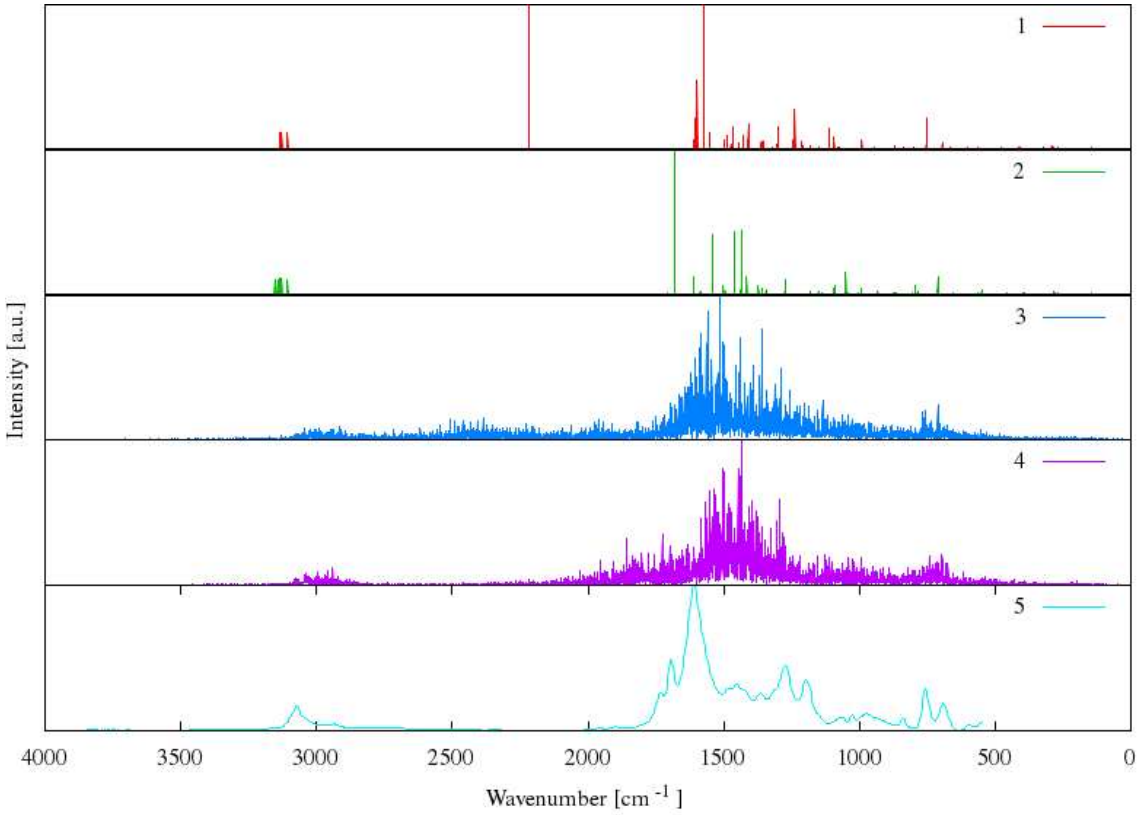

Figure 11. Comparison of the experimental and simulated IR spectra for benzoylacetone in the solid state. The numbers of spectra were assigned as follows: (1) benzoylacetone and (2) dideuterobenzoylacetone in the solid state from the DFT (PBE) harmonic calculation with London-type empirical correction for dispersion interactions, (3) benzoylacetone and (4) dideuterobenzoylacetone in the solid state from CP molecular dynamics simulation at 300 K and number (5) experimental IR absorbance spectrum [53, 54] for the benzoylacetone in the solid.

Table 1. Calculated selected geometrical parameters after optimization compared with the average geometrical parameters from CPMD (standard deviation in brackets) and the existing experimental data for benzoylacetone **(I)** and dideuterobenzoylacetone **(II)** crystals (bond lengths and unit cell parameters are in Å, angles and dihedrals in degrees).

Parameter	PBE / pob_TZVP_2012	PBE / PCG / 80 Ry	CPMD Avg.				Exptl.[24-26]	
			80 Ry / 160 K		80 Ry /300K			
			I	II	I	II	I	II
O1-O2	2.451	2.427	2.493 (0.071)	2.498 (0.069)	2.511 (0.103)	2.515 (0.100)	2.502	2.522
O2-H1 / O2-D1	1.069	1.073	1.164 (0.195)	1.161 (0.198)	1.225 (0.233)	1.205 (0.234)	1.245	1.002
H1…O1 / D1…O1	1.450	1.405	1.404 (0.220)	1.416 (0.224)	1.372 (0.277)	1.397 (0.269)	1.329	1.611
O1-C2	1.286	1.277	1.286 (0.029)	1.285 (0.029)	1.290 (0.365)	1.290 (0.036)	1.286	1.290
O2-C4	1.336	1.324	1.319 (0.029)	1.319 (0.029)	1.316 (0.037)	1.316 (0.037)	1.293	1.293
C2-C3	1.418	1.426	1.416 (0.028)	1.416 (0.028)	1.415 (0.035)	1.415 (0.036)	1.414	1.403
C4-C3	1.388	1.392	1.400 (0.026)	1.399 (0.027)	1.406 (0.034)	1.406 (0.034)	1.405	1.403
C2-C1	1.494	1.492	1.500 (0.024)	1.501 (0.025)	1.503 (0.033)	1.503 (0.033)	1.499	1.493
C4-C5	1.462	1.473	1.475 (0.023)	1.474 (0.023)	1.477 (0.032)	1.477 (0.031)	1.483	1.482
C5-C6	1.408	1.402	1.409 (0.020)	1.409 (0.019)	1.411 (0.027)	1.411 (0.028)	1.406	
C6-C7	1.389	1.394	1.397 (0.019)	1.396 (0.019)	1.398 (0.026)	1.403 (0.026)	1.402	
C7-C8	1.395	1.397	1.395 (0.019)	1.395 (0.019)	1.396 (0.026)	1.396 (0.026)	1.387	
C8-C9	1.395	1.390	1.397 (0.019)	1.397 (0.018)	1.398 (0.026)	1.399 (0.026)	1.404	
C9-C10	1.389	1.396	1.396 (0.019)	1.395 (0.018)	1.397 (0.026)	1.397 (0.026)	1.394	
C10-C5	1.403	1.406	1.402 (0.019)	1.402 (0.019)	1.403 (0.027)	1.403 (0.026)	1.404	
C3-H5 / C3-D5	1.084	1.081	1.083 (0.021)	1.084 (0.020)	1.085 (0.028)	1.085 (0.028)	1.076	
C1-H9	1.099	1.102	1.101 (0.022)	1.100 (0.022)	1.103 (0.031)	1.103 (0.030)	1.064	
C1-H10	1.096	1.093	1.101 (0.022)	1.101 (0.023)	1.102 (0.031)	1.102 (0.030)	1.062	
C1-H11	1.094	1.091	1.100 (0.022)	1.100 (0.022)	1.103 (0.031)	1.103 (0.030)	1.051	
C6-H12	1.091	1.089	1.086 (0.021)	1.085 (0.020)	1.087 (0.028)	1.087 (0.028)	1.079	
C7-H13	1.089	1.085	1.090 (0.021)	1.091 (0.022)	1.093 (0.030)	1.092 (0.029)	1.090	
C8-H14	1.090	1.088	1.093 (0.022)	1.093 (0.021)	1.094 (0.029)	1.094 (0.029)	1.091	
C9-H15	1.088	1.087	1.083 (0.021)	1.085 (0.020)	1.087 (0.028)	1.087 (0.028)	1.090	
C10-H16	1.088	1.085	1.086 (0.022)	1.086 (0.022)	1.088 (0.029)	1.088 (0.029)	1.085	
< O1-H1-O2 / < O1-D1-O2	153.07	156.67	152.03 (4.91)	154.49 (4.87)	150.76 (6.89)	150.53 (6.90)	152.36	148.84
< H1-O2-C4 / < D1-O2-C4	104.89	103.12	103.88 (3.07)	104.14 (3.05)	103.71 (4.15)	103.83 (4.10)	103.24	108.73
< H1-O1-C2 / < D1-O1-C2	100.72	100.25	100.87 (3.11)	100.83 (3.09)	101.07 (4.10)	101.00 (4.10)	101.24	106.73
< O2-C4-C3	119.44	119.74	119.98 (1.98)	120.02 (1.95)	120.02 (2.69)	120.05 (2.71)	120.93	121.21
< O1-C2-C3	121.29	120.87	121.49 (2.05)	121.58 (2.03)	121.51 (2.74)	121.57 (2.78)	122.13	122.4
< C4-C3-C2	120.09	119.20	120.29 (2.05)	120.39 (2.03)	120.45 (2.78)	120.55 (2.81)	120.93	120.3

< C4-C3-H5 / < C4-C3-D5	120.69	121.36	120.30 (3.06)	120.25 (3.01)	120.05 (4.19)	120.10 (4.07)	121.54	
< C2-C3-H5 / < C2-C3-D5	119.01	119.42	118.93 (2.98)	118.88 (2.99)	118.66 (4.13)	118.55 (4.02)	118.74	
< O1-C2-C1	118.27	118.15	118.26 (2.83)	118.38 (2.83)	117.92 (3.64)	117.89 (3.75)	117.03	116.8
< C2-C1-H9	108.12	110.16	110.21 (3.46)	109.96 (3.49)	110.26 (4.76)	110.12 (4.68)	109.84	
< C2-C1-H10	108.83	108.79	109.73 (3.93)	110.37 (3.59)	110.09 (4.64)	110.27 (4.65)	110.84	
< C2-C1-H11	111.72	111.66	110.82 (3.53)	110.42 (3.53)	110.36 (4.72)	110.46 (4.68)	112.65	
< C1-C2-C3	120.43	120.98	120.09 (3.03)	119.88 (2.98)	120.28 (3.94)	120.23 (3.93)	120.92	120.8
< C3-C4-C5	124.90	125.03	122.89 (2.58)	122.79 (2.59)	122.42 (3.28)	122.53 (3.33)	122.62	122.81
< O2-C4-C5	115.65	115.23	116.93 (2.52)	116.99 (2.59)	117.25 (3.21)	117.11 (3.30)	116.43	116.01
< C4-C5-C6	119.93	118.87	119.87 (2.26)	119.95 (2.23)	122.42 (3.28)	119.95 (3.01)	121.52	
< C4-C5-C10	120.87	121.88	121.34 (2.21)	121.31 (2.19)	121.32 (2.98)	121.30 (2.93)	119.02	
< C5-C6-C7	120.32	120.43	120.26 (1.82)	120.24 (1.86)	119.94 (3.01)	120.22 (2.48)	119.83	
< C5-C10-C9	120.04	119.86	120.71 (1.87)	120.79 (1.90)	120.83 (2.53)	120.83 (2.54)	120.32	
< C6-C7-C8	120.09	119.91	120.37 (1.87)	120.41 (1.90)	120.40 (2.56)	120.39 (2.57)	120.43	
< C10-C9-C8	120.53	120.40	120.10 (1.84)	120.04 (1.88)	120.02 (2.54)	119.95 (2.52)	119.93	
< C7-C8-C9	119.82	119.98	119.49 (1.87)	119.49 (1.85)	119.33 (2.52)	119.38 (2.54)	120.13	
< C8-C9-C10	120.53	120.40	120.10 (1.84)	119.49 (1.85)	119.33 (2.53)	119.95 (2.52)	119.93	
< C5-C10-H16	120.79	121.06	120.18 (2.85)	120.10 (2.83)	120.05 (3.69)	120.08 (3.93)	119.14	
< C5-C6-H12	119.22	119.05	119.19 (2.96)	119.24 (2.94)	119.02 (4.07)	119.04 (4.08)	120.94	
< H12-C6-C7	120.45	120.53	120.28 (2.96)	120.25 (2.98)	120.23 (4.12)	120.25 (4.14)	119.24	
< H16-C10-C9	119.13	119.07	118.83 (2.84)	118.82 (2.81)	118.63 (3.99)	118.59 (3.89)	120.64	
< H13-C7-C6	119.53	119.43	119.52 (2.96)	119.48 (2.88)	119.47 (4.01)	119.58 (4.02)	119.04	
< H15-C9-C10	119.19	119.32	119.46 (2.97)	119.49 (2.96)	119.36 (4.07)	119.35 (4.07)	119.74	
< H13-C7-C8	120.36	120.65	119.86 (2.97)	119.86 (2.86)	119.68 (3.94)	119.57 (4.00)	120.64	
< H15-C9-C8	120.28	120.28	120.13 (2.98)	120.17 (2.98)	120.09 (4.05)	119.91 (4.04)	120.44	
< C7-C8-H14	118.90	120.40	120.02 (2.95)	120.02 (2.90)	119.98 (3.99)	119.91 (4.04)	120.74	
< C9-C8-H14	121.27	119.59	120.22 (2.97)	120.24 (2.93)	120.23 (4.04)	120.24 (4.08)	119.24	
ϕ O2-C4-C5-C6	-174.39	-176.07	-173.74 (3.25)	-173.41 (3.25)	-173.02 (3.87)	-173.43 (3.26)	-173.54	-173.72
ϕ H9-C1-C2-O1	37.99	29.85	32.56 (4.18)	33.04 (4.12)	35.02 (4.25)	37.22 (4.03)	38.05	38.45
ϕ H11-C1-C2-O1	-80.87	-88.50	-84.06 (3.56)	-87.23 (3.52)	-83.45 (3.78)	-84.02 (3.25)	-81.06	-82.07
a	7.265						8.028	8.015
b	5.317						5.483	5.485
c	18.694						19.478	19.462
α	90.00						90.00	90.00
β	107.24						110.42	110.34
γ	90.00						90.00	90.00

Table 2. Comparison of the experimental and calculated selected vibrational frequencies in (cm^{-1}) for the crystals **(I)** and **(II)**.

Assignment frequencies	PBE/pob_TZVP_2012 (I) / (II)	CPMD/PBE/80 Ry (I) / (II)	Exptl. [53] (I) / (II)
υ CH / υ CD	3186 / 2361	3107 / 2336	3110 [b] / 2313 [b]
υ $CH_{ring\ assym.}$	3153 / 3152	3023 / 3015	3070 [b] / 3090 [b]
υ $CH_{ring\ symm.}$	3136 / 3136	2995 / 3006	3070 [b] /3070 [b]
υ CH	3128 / 3128	2984 / 2978	3055 [b] / 3055 [b]
υ CH	3114 / 3114	2956 / 2937	3030 [b] / 3030 [b]
υ $CH_{3\ assym.}$	3072 / 3071	2916 / 2895	3000 [b] / 3000 [b]
υ $CH_{3\ symm.}$	2986 / 2988	2892 / 2856	2920 [b] / 2920 [b]
υ OH / υ OD	2217 / 1681	2514 / 1922	2650 [b] / 1960 [b]
υ C=O-C=C + δ OH + δ CH / υ C=O-C=C + δ OD + δ CH	1608 / 1541	1624 / 1546	1620 [a] 1618 [b] / 1525 [b]
δ OH + υ C=O-C=C / δ OD + υ C=O-C=C	1605 / 1540	1609 / 1511	1600 [a] 1605 [b] / 1516 [b]
υ C=C + δ OH / υ C=C + δ OD	1597 / 1461	1579 / 993	1570 [a] 1572 [b] / 1098 [b]
υ C=C + δ OH / υ C=C + δ OD	1572 / 1433	1552 / 969	1555 [a] 1554 [b] / 1098 [b]
δ CH_3 + δ CH + υ C-C=C-O	1497 / 1415	1465 / 1320	1458 [a] 1458 [b] / 1362 [b]
δ CH_3	1443 / 1433	1423 / 1407	1430 [b] / 1430 [b]
υ C-O + δ OH + δ CH_3 / υ C-O + δ OD + δ CH_3	1408 / 1343	1412 / 1073	1430 [b] / 1135 [b]
υ C-C=C + δ OH / υ C-C=C + δ OD	1299 / 1072	1284 / 991	1280 [a] 1272 [b] / 1070 [b]
γ OH / γ OD	1109 / 1050	930 / 702	955 [a] 957 [b] / 720 [b]
ρ CH_3	991 / 989	960 / 910	985 [a] 987 [b] / 890 [b]
γ CH / γ CD	749 / 710	774 / 648	805 [a] 801 [b] / 815 [b]
γ CH_{ring}	695 / 670	691 / 642	764 [a] 770 [b] / 720 [b]
γ C-CH_3	556 / 549	561 / 550	588 [a] 588 [b] / -
νO…O + δ C-CH_3	410 / 395	345 / 279	396 [a] 396 [b] / 384 [b]
γ C-CH_3	152 / 150	161 / 162	153 [a] / 143 [b]
τ CH_3	147 / 144	136 / 140	138 [a] / 143 [b]

Experimental data from Ref. 53 [a] IR of BA in solid state, [b] IR of BA in CCl_4 solution.

Supplementary materials

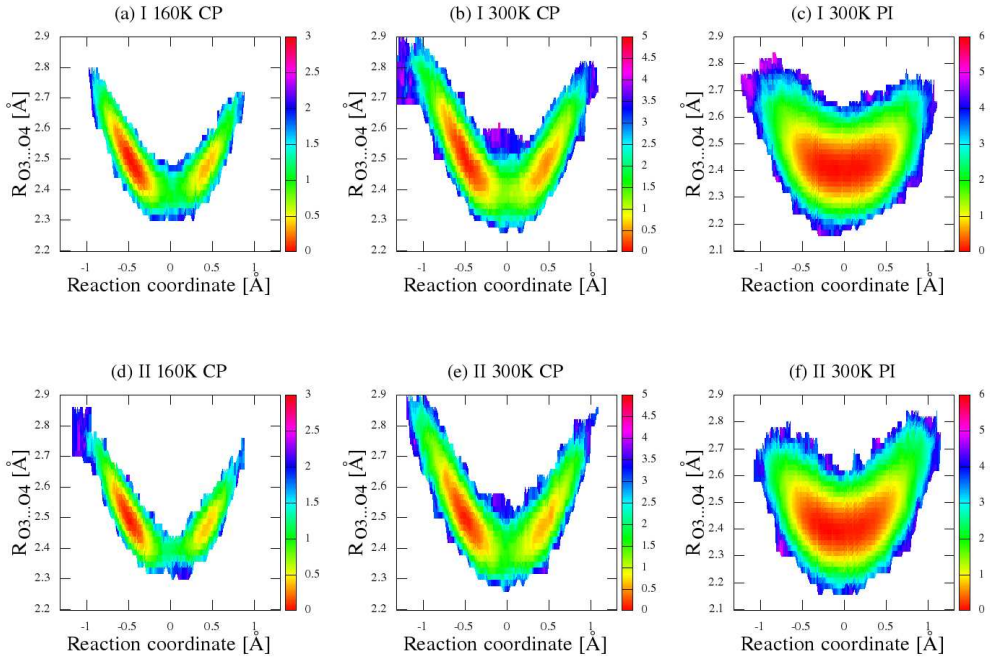

Figure 1S. Two-dimensional free-energy landscape of δ-parameter (reaction coordinate) and $R_{O3...O4}$ distances for crystal **(I)** for (a) CPMD simulation at 160 K, (b) CPMD simulation at 300 K, (c) PIMD simulation at 300 K, and for crystal **(II)** for (d) CPMD simulation at 160 K, (e) CPMD simulation at 300 K, (f) PIMD simulation at 300 K. The unit of ΔF free energy (potential of mean force) is kcal/mol.

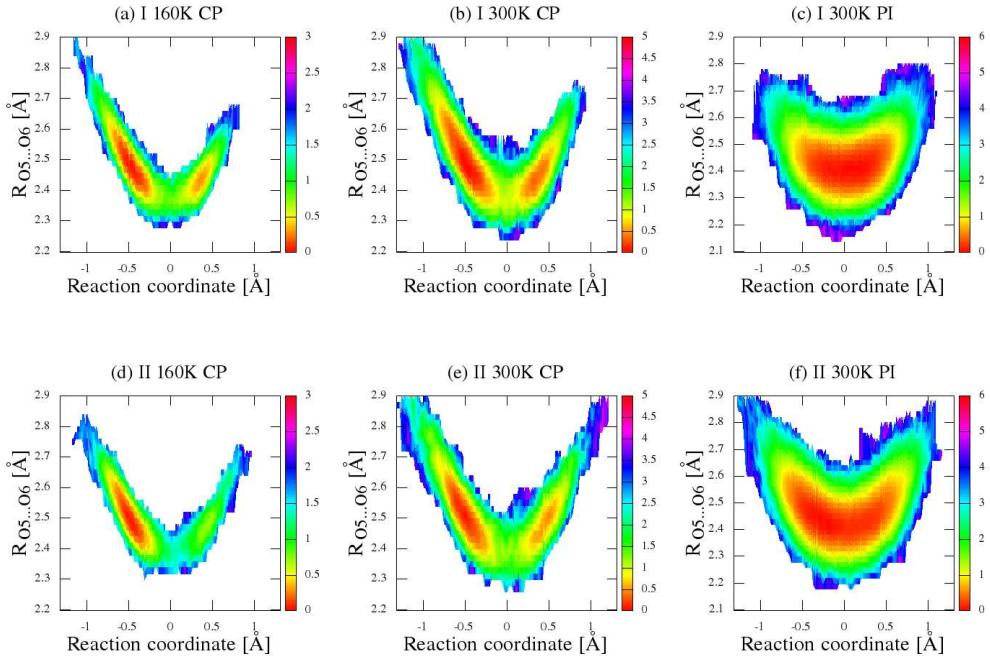

Figure 2S. Two-dimensional free-energy landscape of δ-parameter (reaction coordinate) and $R_{O5...O6}$ distances for crystal **(I)** for (a) CPMD simulation at 160 K, (b) CPMD simulation at 300 K, (c) PIMD simulation at 300 K, and for crystal **(II)** for (d) CPMD simulation at 160 K, (e) CPMD simulation at 300 K, (f) PIMD simulation at 300 K. The unit of ΔF free energy (potential of mean force) is kcal/mol.

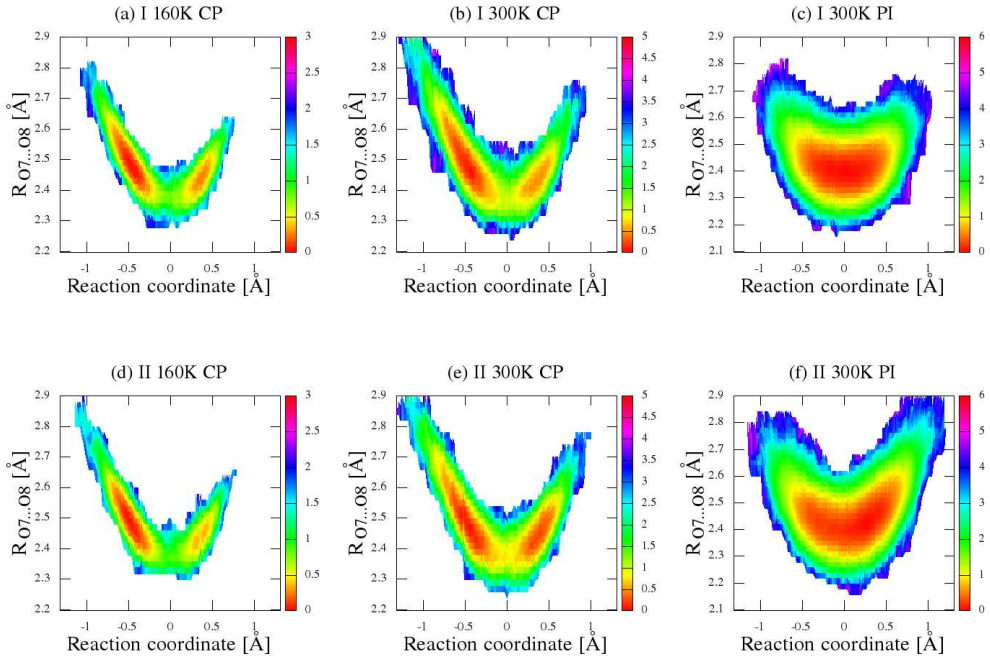

Figure 10. Two-dimensional free-energy landscape of δ-parameter (reaction coordinate) and $R_{O7...O8}$ distances for crystal **(I)** for (a) CPMD simulation at 160 K, (b) CPMD simulation at 300 K, (c) PIMD simulation at 300 K, and for crystal **(II)** for (d) CPMD simulation at 160 K, (e) CPMD simulation at 300 K, (f) PIMD simulation at 300 K. The unit of ΔF free energy (potential of mean force) is kcal/mol.